Second-order quadrupole-shielding effects in magic-angle spinning solid-state nuclear magnetic resonance

Sungsool Wi
Department of Chemistry, University of California, Berkeley, California 60607

Sharon E. Ashbrook and Stephen Wimperis[a)]
School of Chemistry, University of Exeter, Exeter EX4 4QD, United Kingdom

Lucio Frydman
Department of Chemical Physics, Weizmann Institute of Sciences, 76100 Rehovot, Israel

(Received 3 September 2002; accepted 1 November 2002)

We investigate the nature of higher-order effects arising in solid-state nuclear magnetic resonance (NMR) when quadrupolar nuclei are subject to significant chemical shift anisotropies. It is shown that the quadrupole interaction can give rise to shielding-derived terms that are not entirely averaged away by conventional magic-angle spinning (MAS). These terms are proportional to the square of the z component of the spin angular momentum and therefore leave unaffected both the central and other $-m_I \leftrightarrow +m_I$ symmetric multiple-quantum transitions, yet lead to noticeable effects when monitoring other nonsymmetric transitions within the spin manifold. The recently-developed satellite-transition (ST) MAS NMR method for the simultaneous averaging of the first- and second-order quadrupole effects makes such quadrupole-shielding cross-terms observable. Although this may present a resolution limitation to this averaging scheme, it opens up new possibilities for determining the coupling parameters of the quadrupolar nucleus—particularly the relative orientation between its quadrupole and shielding tensors. Average Hamiltonian derivations of these effects are explored, and employed to derive analytical expressions for their resulting splittings. These predictions are then successfully compared with variable-field STMAS NMR spectra of a ^{59}Co-containing sample. A brief discussion of potential complications arising from third-order quadrupole effects when trying to analyze such line shapes is also presented. © *2003 American Institute of Physics.* [DOI: 10.1063/1.1531998]

I. INTRODUCTION

The chemical shift is one of the most valuable observables in nuclear magnetic resonance (NMR).[1] This interaction is described by an isotropic component reflecting the average electronic environment surrounding a chemical site, and by an anisotropic contribution reflecting the orientation of the site with respect to the external magnetic field.[2] The first of these contributions separates inequivalent resonances according to chemical nature while the second, which is directly observable only in solid and liquid-crystalline phases, provides additional electronic and dynamic information about the system under study. Most solid-state NMR spectra, however, are recorded with the aid of averaging techniques such as magic-angle spinning (MAS),[3,4] which sacrifice the anisotropic shielding information at the expense of spectral resolution. Nevertheless, the usefulness of the chemical shift anisotropy (CSA) information has led to a number of one- and two-dimensional spin-1/2 NMR approaches capable of yielding this information in a high-resolution format.[5] The principle of such methods is to combine MAS with other types of spin or spatial manipulations, so as to reintroduce in an active fashion the inhomogeneous evolution associated with the shift anisotropies. Although not widely appreciated, the possibility arises in certain areas of solid-state NMR of encountering CSA-derived effects that cannot be entirely removed by fast MAS. One such instance arises when nuclei with spin quantum numbers $I>1/2$ are involved. As shown in further detail in the following, the tilting of the axis of spin quantization brought about by quadrupolar interactions can result in significant second-order quadrupole-shielding effects that will be scaled but not entirely removed by conventional MAS.

Although generally harder to detect than their first-order counterparts, the experimental observation of higher-order NMR effects such as that described in the previous paragraph is not uncommon.[6,7] Perhaps the best known example involves second-order quadrupole–quadrupole effects, which largely dominate the central-transition spectroscopy of half-integer quadrupole nuclei.[8,9] Another well-documented case is that of the residual dipolar splittings that can be observed, even under fast MAS, when a nucleus is dipole-coupled to an $S>1/2$ spin (e.g., in ^{13}C–^{14}N spin pairs).[10–12] The quadrupole-shielding effects that concern us here have been discussed recently in the context of single-crystal NMR and have been shown to lead to anisotropies whose magnitudes are of the order of 10^{-6} of the quadrupole coupling constant and hence measurable under moderate-to-strong quadrupole and shielding coupling conditions.[13] They have also been noticed in certain recent high-resolution measurements on

[a)]Electronic mail: s.wimperis@exeter.ac.uk

^{14}N, a spin-1 nucleus.[14] The present paper further discusses hitherto unexplored aspects of these quadrupole-shielding cross terms, focusing in particular on their potential application to the measurement of CSA components from the MAS spectra of half-integer quadrupole nuclei. As a basis for such an analysis, we introduce in Sec. II the perturbative Hamiltonian describing these second-order quadrupole-shielding effects. The resulting expressions suggest that these new effects can be discerned in the satellite-transition line shapes, provided that the larger first- and second-order quadrupolar anisotropies that dominate these transitions are removed first. This can be carried out with the aid of the recently proposed two-dimensional satellite-transition MAS (STMAS) NMR experiment,[15,16] which when implemented on an octahedral cobalt complex yields ^{59}Co NMR spectra displaying the expected broadenings.

II. HIGH-FIELD DESCRIPTION OF QUADRUPOLE-SHIELDING EFFECTS UNDER MAS

Although the line shape distortions arising from quadrupole-shielding cross terms could in principle be computed by numerical diagonalizations of the complete laboratory-frame Hamiltonian, it is illustrative to consider their description within a perturbative setting. This will result in general analytical expressions that yield valuable insight about these effects, as well as aiding the development of experiments for measuring them. Furthermore, given the relatively small coupling magnitudes involved, it can be shown that for most cases of interest a perturbative description of quadrupole-shielding effects will be sufficient for a complete description of their spectral consequences.

To derive an analytical form for the second-order quadrupolar-shielding perturbative Hamiltonian we follow a notation akin to that in Ref. 17, and begin by considering the full laboratory-frame Hamiltonian for a single quadrupolar spin $I>1/2$:

$$H_{\mathrm{lab}}=H_Z+H_Q+H_{\mathrm{CS}}. \tag{1}$$

Here H_Z is the dominant Zeeman coupling of the spin with the external magnetic field, H_Q is its quadrupolar interaction, and H_{CS} its chemical shift interaction. These various laboratory-frame Hamiltonians can be described using irreducible spherical tensor spin and spatial operators as

$$\begin{aligned} H_Z&=-\gamma B_0 I_z=-\omega_0 T_{1,0},\\ H_Q&=\sum_{m=-2}^{2}(-1)^m T^Q_{2,-m}R^Q_{2,m},\\ H_{\mathrm{CS}}&=\omega_0\sigma_{\mathrm{iso}}T_{1,0}+\sum_{l=1}^{2}\sum_{m=-2}^{2}(-1)^m T^{\mathrm{CS}}_{l,-m}R^{\mathrm{CS}}_{l,m}, \end{aligned} \tag{2}$$

leading to an explicit laboratory-frame form

$$\begin{aligned} H_{\mathrm{lab}}=&-\omega_0(1-\sigma_{\mathrm{iso}})I_z+\chi_Q\Big[R^Q_{2,0}\{3I_z^2-I(I+1)\}\\ &+\sqrt{\frac{3}{2}}(R^Q_{2,-2}I_+^2-R^Q_{2,-1}\{I_zI_++I_+I_z\}\\ &+R^Q_{2,1}\{I_zI_-+I_-I_z\}+R^Q_{2,2}I_-^2)\Big]+B_0\Big[\sqrt{\frac{2}{3}}R^{\mathrm{CS}}_{2,0}I_z\\ &+\frac{1}{2}(R^{\mathrm{CS}}_{2,-1}I_+-R^{\mathrm{CS}}_{2,1}I_-+R^{\mathrm{CS}}_{1,-1}I_++R^{\mathrm{CS}}_{1,1}I_-)\Big]. \end{aligned} \tag{3}$$

In these equations $\omega_0=\gamma B_0$ is the Larmor frequency, σ_{iso} denotes the isotropic shielding, $\chi_Q=eQ/[2I(2I-1)\hbar]$ is a parameter representing the nuclear quadrupole moment, and the last term describes the anisotropic contribution from the chemical shielding interaction in terms of its symmetric and antisymmetric components. The spherical tensor elements $\{R^\lambda_{l,m}\}_{\lambda=Q,\mathrm{CS}}$ involved in these various Hamiltonians can be related to further coupling parameters via a series of consecutive transformations from their respective principal axis systems (PAS) into a common laboratory reference frame. The focus in the present work will be on MAS NMR experiments, where such transformations are usually defined via an intermediate rotor-based frame as

$$\mathrm{CS}\xrightarrow{\Omega_1=(\alpha,\beta,\gamma)}Q\xrightarrow{\Omega_2=(\varphi,\theta,\xi)}\mathrm{ROTOR}\xrightarrow{\Omega_3=(\omega_r,t,54.736^\circ,0^\circ)}\mathrm{LAB}. \tag{4}$$

The explicit relations between the principal elements $\{\rho^\lambda_{l,m}\}$ and their spatial counterparts in a general frame $\{R^\lambda_{l,m}\}$ then become

$$R^Q_{2,m}=\sum_{k=-2}^{2}\sum_{n=-2}^{2}D^2_{k,m}(\omega_r t,54.736^\circ,0^\circ)D^2_{n,k}(\varphi,\theta,\xi)\rho^Q_{2,n} \tag{5}$$

and

$$\begin{aligned} R^{\mathrm{CS}}_{l,m}=&\sum_{k=-2}^{2}\sum_{n=-2}^{2}\sum_{p=-2}^{2}D^2_{k,m}(\omega_r t,54.736^\circ,0^\circ)\\ &\times D^2_{n,k}(\varphi,\theta,\xi)D^2_{p,n}(\alpha,\beta,\gamma)\rho^{\mathrm{CS}}_{l,p}, \end{aligned} \tag{6}$$

where we have used the usual definitions[18,19]

$$\rho^Q_{2,0}=\frac{1}{2}eq,\quad \rho^Q_{2,\pm1}=0,\quad \rho^Q_{2,\pm2}=\frac{eq}{2\sqrt{6}}\eta_Q, \tag{7}$$

$$\begin{aligned} &\rho^{\mathrm{CS}}_{1,0}=-\sqrt{2}i\gamma\sigma^a_{XY},\quad \rho^{\mathrm{CS}}_{1,\pm1}=\gamma(\sigma^a_{XZ}\pm i\sigma^a_{YZ}),\\ &\rho^{\mathrm{CS}}_{2,0}=\sqrt{\frac{3}{2}}\gamma\sigma_{\mathrm{CSA}},\quad \rho^{\mathrm{CS}}_{2,\pm1}=0,\quad \rho^{\mathrm{CS}}_{2,\pm2}=\frac{\eta_{\mathrm{CS}}\gamma\sigma_{\mathrm{CSA}}}{2}. \end{aligned} \tag{8}$$

The actual extension of these expressions to the case of static samples ($\omega_r=0$) is straightforward and will not be presented here.

Insight into the various first- and second-order effects that H_Q and H_{CS} will give rise to can be obtained by treating these Hamiltonians as perturbations to the dominant Zeeman term. A common approach to calculating progressive perturbations in this high-field regime is average Hamiltonian

theory, which calculates the perturbations by transforming each H_λ in Eq. (2) into an interaction representation driven by the Zeeman propagator $U(t)=\exp[i\omega_0 I_z t]$. This imparts into each H_λ the time dependence

$$\tilde{H}_\lambda(t)=U(t)\cdot H_\lambda\cdot U^{-1}(t)+\frac{dU(t)}{dt}U^{-1}(t). \tag{9}$$

A time-independent rendering of these rotating-frame interactions can then be derived according to[2,8,19]

$$\bar{H}=\sum_\lambda H_\lambda^{(1)}+\sum_{\lambda,\lambda'} H_{\lambda,\lambda'}^{(2)},+\cdots, \tag{10}$$

where

$$H_\lambda^{(1)}=\frac{1}{\tau_c}\int_0^{\tau_c}\tilde{H}_\lambda(t)dt, \tag{11}$$

$$H_{\lambda,\lambda'}^{(2)}=\frac{-i}{2\tau_c}\int_0^{\tau_c}dt\int_0^t[\tilde{H}_\lambda(t),\tilde{H}_{\lambda'}(t')]dt' \tag{12}$$

are average perturbations over the $\tau_c=2\pi/\omega_0$ Larmor period. From among all these terms, it is usually sufficient to consider the first-order Hamiltonian for the chemical shift, plus the first- and second-order terms for the quadrupolar coupling. This leads to the well-known expressions

$$H_{\mathrm{CS}}^{(1)}=\left(\sigma_{\mathrm{iso}}\omega_0+\sqrt{\frac{2}{3}}B_0R_{2,0}^{\mathrm{CS}}\right)I_z, \tag{13}$$

$$H_Q^{(1)}=\chi_Q R_{2,0}^Q\{3I_z^2-I(I+1)\}, \tag{14}$$

and

$$H_{Q,Q}^{(2)}=\frac{3}{\omega_0}\chi_Q^2\{R_{2,-1}^Q R_{2,1}^Q I_z[4I(I+1)-8I_z^2-1] + R_{2,-2}^Q R_{2,2}^Q I_z[2I(I+1)-2I_z^2-1]\}. \tag{15}$$

In the present study, however, we will also assume that the quadrupolar and shielding couplings are large enough to warrant consideration of $H_{Q,\mathrm{CS}}^{(2)}$, the second-order term arising from quadrupole-shielding effects. This term can be derived on the basis of Eq. (12) as

$$H_{Q,\mathrm{CS}}^{(2)}=-\sqrt{\frac{3}{2}}\chi_Q\frac{B_0}{\omega_0}[(R_{2,1}^Q R_{2,-1}^{\mathrm{CS}}+R_{2,-1}^Q R_{2,1}^{\mathrm{CS}}) + (R_{2,1}^Q R_{1,-1}^{\mathrm{CS}}-R_{2,-1}^Q R_{1,1}^{\mathrm{CS}})][3I_z^2-I(I+1)]. \tag{16}$$

This interaction is written as the sum of cross terms $\{R_{2,m}^Q R_{2,-m}^{\mathrm{CS}}\}$ between nonsecular quadrupolar and symmetric shielding components, plus cross terms involving the antisymmetric shielding terms $\{R_{2,m}^Q R_{1,-m}^{\mathrm{CS}}\}$. The second-order term $H_{Q,\mathrm{CS}}^{(2)}$ thus exhibits the basic features mentioned in Sec. I: it is of the order of 10^{-6} of the quadrupolar coupling and is independent of the external magnetic field strength, and it involves products of second-rank spatial components which are known to be beyond the averaging capabilities of conventional MAS.[20,21]

To further explore the nature of this interaction upon subjecting the sample to MAS, we focus on the averaged centerbands that can be expected in either fast-spinning or rotor-synchronized experiments. This avenue, similar to that employed for deriving analytical high-field expressions in the case of heteronuclear quadrupole-dipole cross terms,[11,12,22] requires calculating for all spatial terms in the Hamiltonian the rotor-period average

$$\langle H_{Q,\mathrm{CS}}^{(2)}\rangle=\frac{\omega_r}{2\pi}\int_0^{2\pi/\omega_r}H_{Q,\mathrm{CS}}^{(2)}(t)dt. \tag{17}$$

On implementing such rotor averaging it is found that the antisymmetric contribution $\langle R_{2,1}^Q R_{1,-1}^{\mathrm{CS}}-R_{2,-1}^Q R_{1,1}^{\mathrm{CS}}\rangle$ vanishes, leaving for $\langle H_{Q,\mathrm{CS}}^{(2)}\rangle$ eigenvalues of the form

$$\langle E(m_I)\rangle_{Q,\mathrm{CS}}=-\sqrt{\frac{3}{2}}\chi_Q\frac{B_0}{\omega_0}\langle R_{2,1}^Q R_{2,-1}^{\mathrm{CS}}+R_{2,-1}^Q R_{2,1}^{\mathrm{CS}}\rangle \times[3m_I^2-I(I+1)]. \tag{18}$$

The resulting equation can be computed numerically to retrieve the residual shielding effects for arbitrary coupling conditions. In addition it can be employed to obtain, from its powder average over all possible $\Omega_2=(\varphi,\theta,\xi)$ orientations within a solid sphere, the center-of-mass that will arise from this effect for arbitrary spin transitions. This entails removing the anisotropic dependencies still remaining in Eq. (18) by calculating the weighted integral

$$\frac{1}{4\pi}\int_0^{2\pi}\int_0^{\pi}\langle R_{2,1}^Q R_{2,-1}^{\mathrm{CS}}+R_{2,-1}^Q R_{2,1}^{\mathrm{CS}}\rangle\sin\theta d\,\theta d\,\varphi, \tag{19}$$

with the remaining powder angle ξ being irrelevant as it denotes a rotor phase that has already been averaged away by the MAS. The result of implementing such powder integration on the expression for the eigenvalues (Eq. (18)) is the isotropic energy shift (in rad s^{-1})

$$\langle E(m_I)\rangle_{Q,\mathrm{CS}}=\tfrac{3}{20}eq\cdot\chi_Q\cdot\sigma_{\mathrm{CSA}}\cdot\Delta\cdot[3m_I^2-I(I+1)], \tag{20}$$

where the Euler angles between the tensors are collected in the geometric function

$$\Delta=\{3\cos^2\beta-1+\eta_{\mathrm{CS}}\sin^2\beta\cos 2\alpha\} + \eta_Q\left\{\sin^2\beta\cos 2\gamma+\frac{\eta_{\mathrm{CS}}}{3}[(\cos^2\beta+1) \times\cos 2\alpha\cos 2\gamma-2\cos\beta\sin 2\alpha\sin 2\gamma]\right\}. \tag{21}$$

When compared with analogous functions derived for quadrupole–dipole second-order effects,[12,17] this geometric expression shows an identical first term plus an additional one (proportional to η_Q) which arises from considering cross terms between two nonaxially symmetric tensors. These analytical equations can then be used to estimate the net isotropic shift that quadrupole-shielding effects will introduce on any $m_I\leftrightarrow m_I'$ single- or multiple-quantum transition within the $2I+1$ nuclear spin energy levels:

$$\langle\omega(m_I,m_I')\rangle_{Q,\mathrm{CS}}=\frac{9}{20}\cdot\frac{e^2qQ}{2I(2I-1)\hbar}\cdot\sigma_{\mathrm{CSA}}\cdot\Delta\cdot[m_I^2-m_I'^2]. \tag{22}$$

III. RESIDUAL QUADRUPOLE-SHIELDING EFFECTS IN SATELLITE-TRANSITION MAS NMR

Owing to the quadratic dependence characterizing the spin term in Eq. (22), it follows that these second-order interactions will not affect either the central or any other symmetric $-m_I \leftrightarrow +m_I$ transition within the spin manifold. Thus conventional MAS[9,21] or multiple-quantum MAS[23,24] NMR spectra will be free from these line-broadening effects. On the other hand, other forms of MAS correlation spectroscopy involving nonsymmetric transitions, such as double-quantum or satellite-transition NMR, could in principle encode the information that these effects carry. Because of its more widespread character, we address here the effects that $H^{(2)}_{Q,\mathrm{CS}}$ will introduce on the latter STMAS technique, starting with a brief survey of this method. On the basis of this discussion, the analysis of the effects of $H^{(2)}_{Q,\mathrm{CS}}$ on other types of correlation experiment is then straightforward.

As with its MQMAS counterpart, STMAS is a two-dimensional NMR experiment capable of providing high-resolution NMR spectra of half-integer quadrupole nuclei by correlating pairs of transitions within the I-spin manifold. In particular, STMAS correlates the spin evolution of $\pm(m_I - 1 \leftrightarrow m_I)$ satellite-transition frequencies in the ν_1 dimension of the two-dimensional spectrum with $+\frac{1}{2} \leftrightarrow -\frac{1}{2}$ central-transition frequencies in the ν_2 dimension.[15,16] If considering solely quadrupolar and chemical shift interactions, either of these evolution frequencies can be generally written as

$$\begin{aligned}\omega(m_I - 1 \leftrightarrow m_I) = &\{\omega^{\mathrm{CS}}_{\mathrm{iso}} + \omega^{\mathrm{CS}}_{\mathrm{aniso}}(\varphi,\theta)P_2(\cos\psi)\} \\ &+ \omega^{Q}_{\mathrm{aniso}}(\varphi,\theta)C_{20}(m_I)P_2(\cos\psi) \\ &+ \{\omega^{Q}_0 C_0(m_I) \\ &+ \omega^{Q}_2(\varphi,\theta)C_2(m_I)P_2(\cos\psi) \\ &+ \omega^{Q}_4(\varphi,\theta)C_4(m_I)P_4(\cos\psi)\}. \qquad (23)\end{aligned}$$

Here $\omega^{\mathrm{CS}}_{\mathrm{iso}} = \sigma_{\mathrm{iso}}\omega_0$ and $\omega^{\mathrm{CS}}_{\mathrm{aniso}}(\varphi,\theta) = \sqrt{(2/3)}B_0 R^{\mathrm{CS}}_{20}$ are the isotropic and anisotropic chemical shift frequencies, $\omega^{Q}_{\mathrm{aniso}}(\varphi,\theta) = 3\chi_Q R^Q_{20}$ is the first-order quadrupole anisotropy, $C_{20}(m_I) = 2m_I - 1$ weights this first-order anisotropy for each transition, and

$$\begin{aligned}C_0(m_I) &= I(I+1) - 9m_I(m_I-1) - 3, \\ C_2(m_I) &= 8I(I+1) - 36m_I(m_I-1) - 15, \qquad (24) \\ C_4(m_I) &= 18I(I+1) - 102m_I(m_I-1) - 39\end{aligned}$$

scale the zero-, second-, and fourth-rank second-order quadrupole contributions given by

$$\omega^{Q}_0 = \frac{6}{5\omega_0}\chi^2_Q[2R^Q_{2,-1}R^Q_{2,1} - 2R^Q_{2,-2}R^Q_{2,2} - R^Q_{2,0}R^Q_{2,0}],$$

$$\omega^{Q}_2(\varphi,\theta) = \frac{3}{7\omega_0}\chi^2_Q[R^Q_{2,-1}R^Q_{2,1} + 2R^Q_{2,-2}R^Q_{2,2} - R^Q_{2,0}R^Q_{2,0}], \qquad (25)$$

$$\omega^{Q}_4(\varphi,\theta) = \frac{3}{35\omega_0}\chi^2_Q[3R^Q_{2,-1}R^Q_{2,1} + 4R^Q_{2,-2}R^Q_{2,2} + R^Q_{2,0}R^Q_{2,0}].$$

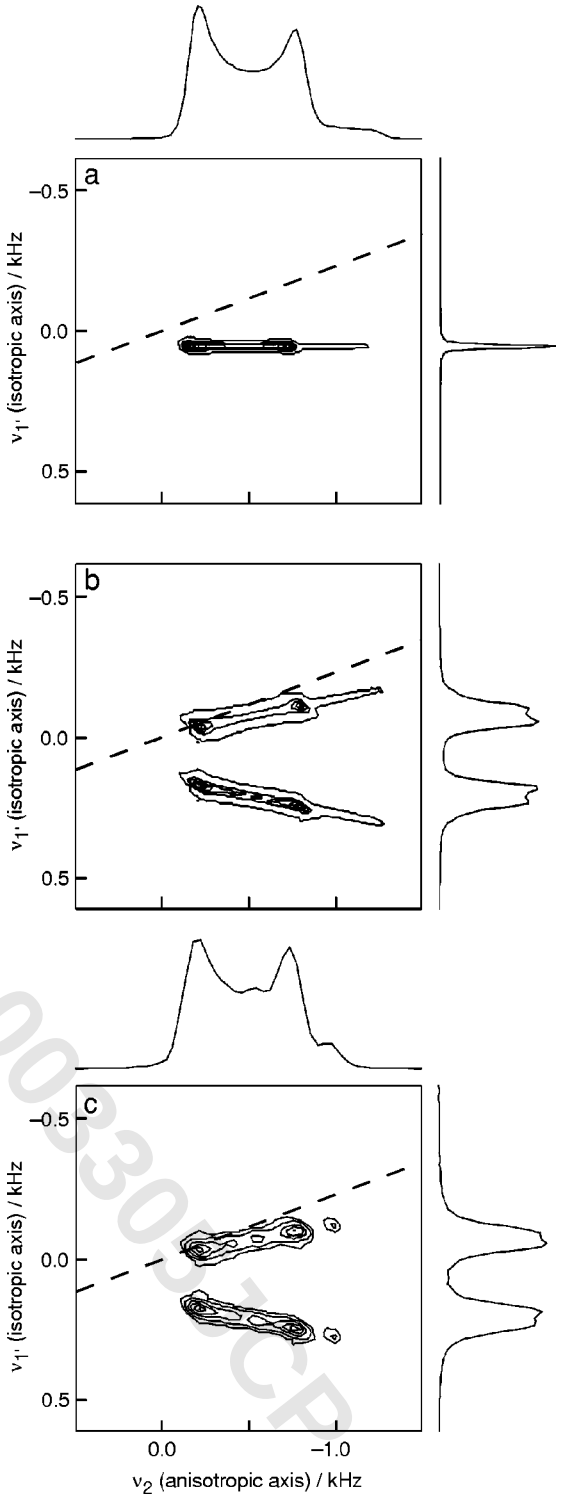

FIG. 1. Comparisons between two-dimensional STMAS NMR spectra expected for a spin $I = 7/2$ nucleus in the absence of CSA effects (a), and upon including second-order quadrupole-shielding interactions (b), (c). The spectrum in (b) was derived from the perturbative expressions given in Eqs. (18)–(25), while (c) results from a "brute-force" propagation of the spin system in the laboratory frame. In each case the innermost correlation $\mathrm{ST}_1(\pm 3/2 \leftrightarrow \pm 1/2) \rightarrow \mathrm{CT}(-1/2 \leftrightarrow +1/2)$ was assumed monitored stroboscopically with the 10 kHz MAS rate, and subject to a shearing transformation that ideally produces an isotropic/second-order quadrupole correlation. For the perturbative-based simulation 200^2 powder orientations were propagated over 256×256 t_1, t_2 points using 100 μs dwell times; for the brute-force calculation 23^3 orientations were propagated in 10 ns time increments over 128×128 points. Other simulation parameters are given in the text. Dashed lines indicate the position of the CT→CT autocorrelation diagonal.

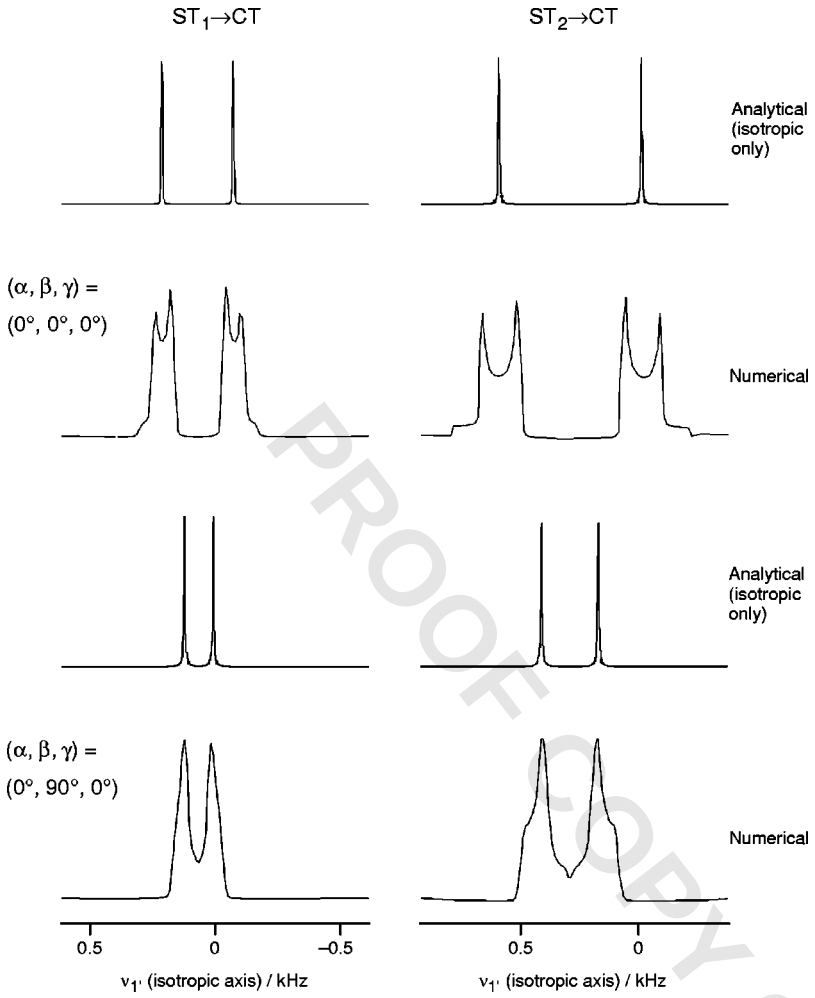

FIG. 2. Comparisons between the ''isotropic'' (actually, anisotropically broadened by quadrupole-shielding cross terms) line shapes resulting from sheared projections of perturbative quadrupole-shielding line shapes such as those illustrated in Fig. 1(b), and stick spectra predicted on the basis of the analytical expression given in Eq. (27). Peak shapes in these analytical traces were artificially broadened to 10 Hz. In each case the coupling parameters were as assumed in Fig. 1, and the correlations considered were $ST_1(\pm 3/2 \leftrightarrow \pm 1/2) \rightarrow CT$ and $ST_2(\pm 5/2 \leftrightarrow \pm 3/2) \rightarrow CT$.

The axis of sample spinning ψ further scales all anisotropies via $P_2(\cos\psi) = (3\cos^2\psi - 1)/2$ and $P_4(\cos\psi) = (35\cos^4\psi - 30\cos^2\psi + 3)/8$. The idea of STMAS is to remove first all second-rank anisotropies by setting ψ exactly at the magic angle and then disregarding the MAS time-modulations by highly accurate rotor-synchronized sampling. All that is then left in terms of anisotropies is the broadening arising from the fourth-rank term. Since the extents to which both satellite and central transitions are affected by this term are proportional for every crystallite in the sample, shearing the resulting two-dimensional NMR data according to

$$S(\nu_{1'}, \nu_2) = S\left(\frac{\nu_1 - \nu_2 R_4(m_I)}{1 + |R_4(m_I)|}, \nu_2\right), \tag{26}$$

where $R_4(m_I) = C_4(m_I)/C_4(1/2)$, provides a purely isotropic high-resolution projection along the $\nu_{1'}$ spectral axis, correlated with the central-transition MAS line shape along the ν_2 axis.

With these considerations at hand, we can proceed to compute the spectral changes that quadrupole-shielding effects can be expected to introduce in STMAS NMR spectra. Toward this end, we consider a hypothetical case incorporating the frequency expressions of Sec. II, and coupling parameters characteristic of a transition-metal isotope:[25] $I = 7/2$, $\omega_0/2\pi = 47.2$ MHz, $e^2qQ/h = 3.1$ MHz, $\delta_{iso} = 0$ ppm, $\delta_{CSA} = 1750$ ppm, $\eta_{CS} = 0.2$, $\eta_Q = 0$, and collinear shielding and quadrupole tensors. Figure 1 shows how the originally sharp isotropic resonance that could otherwise be expected from a sheared, rotor-synchronized STMAS NMR experiment, splits and broadens upon inclusion of the isotropic and anisotropic quadrupole-shielding effects, respectively. Also compared in Fig. 1 are the nearly identical predictions given by a time-incremented diagonalization of the full laboratory-frame Hamiltonian [Eq. (1)] and by the perturbative frequencies stemming from Eq. (16). In fact, we find that in all cases of relevance to STMAS, the high-field approximation provides results that are indistinguishable from the ''brute-force'' laboratory-frame calculations.

Equations (22)–(26) can also be used to calculate analytically the centers of mass characterizing the various satellite-central correlations along the isotropic dimension of STMAS NMR spectra. Considering only the quadrupole-shielding cross terms, and the shearing involved in STMAS, it can be shown that each $m_I - 1 \leftrightarrow m_I$ satellite-central correlation peak will exhibit an isotropic splitting (in Hz) due to quadrupole-shielding effects

$$\Delta\nu_{1'}(m_I - 1 \leftrightarrow m_I) = \frac{9}{10(1 + |R_4(m_I)|)} \cdot \frac{e^2qQ}{2I(2I-1)h} \cdot \sigma_{CSA} \cdot \Delta \cdot (1 - 2m_I). \tag{27}$$

Figure 2 compares the predictions that Eqs. (22)–(27) make

regarding the position of the various peaks appearing along the isotropic STMAS dimension, against numerical simulations resulting from the integration of the $H^{(2)}_{Q,\mathrm{CS}}$ MAS Hamiltonian. As can be appreciated, Eq. (27) describes all the isotropic splitting information arising from the quadrupole-shielding effect on the satellite-central correlations. Note that peaks in the isotropic dimension of STMAS NMR spectra are linear combinations of satellite and central transitions and, since the latter lack quadrupole-shielding splittings, we would expect any isotropic dimension splittings to be scaled down from those found in the pure satellite transitions: this is the origin of the factor $(1+|R_4(m_I)|)^{-1}$ introduced by the shearing transformation into Eq. (27).

These isotropic shifts can in principle be inverted to extract the chemical shift anisotropy information contained in the $\sigma_{\mathrm{CSA}}\cdot\Delta$ parameter. In addition, a potentially valuable feature of the quadrupole-shielding effects lies in the two-dimensional line shapes which will characterize the STMAS multiplets. Indeed, for each resolved chemical site these two-dimensional line shapes should provide additional information about the CSA parameters, and in particular about the often elusive Euler angles relating the orientations of the quadrupolar and CSA coupling tensors. Numerical simulations based on the perturbative model validate such expectations, as presented in Fig. 3 for an $I=7/2$ spin subject to the coupling parameters used in Fig. 1, but this time with $\eta_Q=\eta_{\mathrm{CS}}=1$ and with varying geometries between its two interaction tensors.

Before concluding this section and in view of the relatively small magnitude of the effects being here explored (10^2–10^3 Hz), it is worth considering whether other potential anisotropies could prevent or complicate the measurement of $H^{(2)}_{Q,\mathrm{CS}}$ effects. One such source of broadening is of course of a technical nature, and is the one associated with the stringent experimental conditions demanded by STMAS experiments. Indeed, even minor missettings of the sample spinning axis away from the magic angle or of the MAS rate away from the rate of data digitization may bring the first-order quadrupole interaction into play, thereby introducing considerable broadenings in the spectral lines and smearing the CSA information being sought. Yet even in the absence of this technical complication there are other broadening mechanisms that could potentially spoil the observation of quadrupole-shielding cross terms. One such effect arises from quadrupole-dipole cross terms; these have already been extensively discussed elsewhere[17,26–29] and, if suspected, their consequences could be *a priori* computed. Another potential broadening mechanism arises from third-order quadrupolar effects. Such effects, which have been previously discussed within a static EPR setting and more recently within a NMR one,[30,31] were revisited for this study. Although a more complete description of them will be presented elsewhere, it is sufficient here to mention that under MAS their addition to the $m_I-1\leftrightarrow m_I$ satellite-transition isotropic shift will be given by

$$\langle\omega(m_I-1\leftrightarrow m_I)\rangle_{Q,Q,Q}=\frac{(eq\chi_Q)^3}{\omega_0^2}\left\{\begin{array}{c}\left(-\frac{3}{7}+\frac{893}{1512}\eta_Q^2\right)(1-4m_I+6m_I^2-4m_I^3)\\ \left[+\frac{69}{560}-\frac{607}{7560}\eta_Q^2+\left(\frac{9}{28}-\frac{253}{630}\eta_Q^2\right)I(I+1)\right](1-2m_I)\end{array}\right\}. \tag{28}$$

It can be verified that this shift will leave unaffected the central or other $-m_I\leftrightarrow+m_I$ transitions, while providing for symmetric satellite displacements that are opposite in sign. For the kind of quadrupole couplings and fields being dealt with in this work it can also be checked that these shifts ($\sim$10 Hz) will be an order of magnitude smaller than their second-order quadrupole-shielding counterparts; their details are therefore no longer pursued.

IV. EXPERIMENTAL OBSERVATION OF QUADRUPOLE-SHIELDING EFFECTS

It follows from the above-given arguments that STMAS NMR can be used to monitor CSA parameters through the nonsecular effects induced by quadrupole-shielding cross terms. In order to test this prediction, ^{59}Co, a 100% naturally abundant $I=7/2$ nucleus, was chosen as target. This transition metal nuclide shows the combined benefits of high sensitivity, sizable chemical shielding anisotropies (100–1000 ppm), and moderate nuclear quadrupole moment (0.4 barns). ^{59}Co NMR spectra were obtained at a Larmor frequency of 94.5 MHz on a Bruker Avance 400 spectrometer equipped with a widebore 9.4 T magnet, and at 47.2 MHz on an Avance 200 equipped with a widebore 4.7 T magnet. Powdered samples were packed inside 2.5 mm (Avance 400) and 4 mm (Avance 200) MAS rotors. No line narrowing was evident upon ^{1}H decoupling, hence it was not employed when recording the two-dimensional spectra. ^{59}Co radio-frequency field strengths $\omega_1/2\pi$ between 80 and 120 kHz were used. All ppm scales are referenced relative to 1 M (aq) $K_3[Co(CN)_6]$.

STMAS NMR experiments were recorded using a three-pulse phase-modulated shifted-echo pulse sequence.[32,33] Rotor synchronization or half-rotor synchronization was used in the t_1 period of these experiments by setting the increment equal to the rotor period or half the rotor period, respectively. Owing to the phase problems created by analog filters and the very large number of spinning sidebands, such rotor synchronization was not utilized in the t_2 acquisition period, and only the centerband was observed. The magic angle was set to an estimated accuracy of $54.736°\pm0.004°$, first by opti-

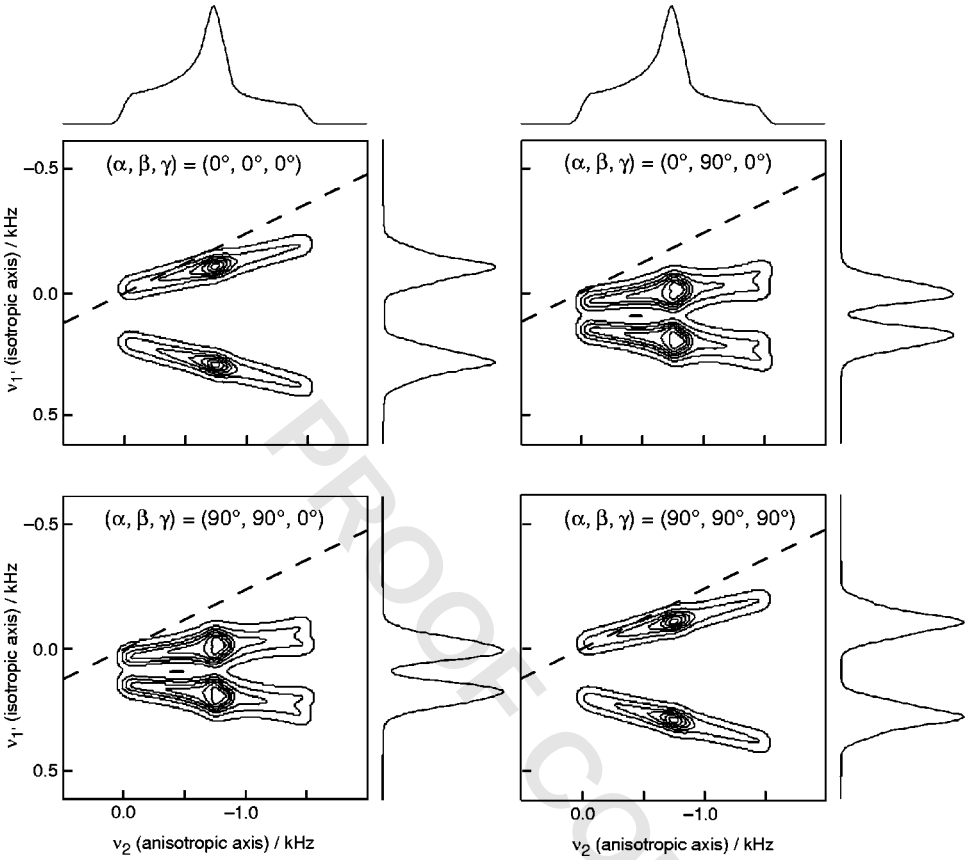

FIG. 3. Expected dependencies of sheared two-dimensional STMAS line shapes on the relative orientations between the quadrupole and shielding coupling tensors. Spectra were calculated for the innermost satellite-transition correlations using the parameters of Fig. 1 (except that $\eta_Q = \eta_{CS} = 1$) and the indicated sets of intertensor Euler angles. Horizontal and vertical spectra correspond to the anisotropic and isotropic projections of the two-dimensional data sets. Dashed lines indicate the position of the CT $\rightarrow$CT autocorrelation diagonal.

mization of the number and intensity and rotary echoes in a normal ^{79}Br KBr signal, and second by maximizing the height of satellite-transition shifted-echo signals in one-dimensional ^{87}Rb STMAS experiments performed on $RbNO_3$.[33] In all cases, the setting of the magic angle was checked both before and after the STMAS experiment, using either ^{87}Rb NMR of $RbNO_3$ or ^{59}Co NMR of sodium hexanitrocobaltate $Na_3Co(NO_2)_6$, to ensure its accuracy. Triple-quantum MAS spectra were obtained using a three-pulse phase-modulated shifted-echo sequence,[34] and were also recorded with rotor-synchronized or half-rotor-synchronized acquisition in the t_1 period.

Figure 4 shows the conventional ^{59}Co MAS NMR spectrum of a sample that is suitable for this type of measurement: cobalt(III) acetylacetonate ($Co(acac)_3$). From previous single-crystal studies the coupling and chemical shift parameters of the sole chemically inequivalent metal site in the unit cell are accurately known:[17,35] $e^2qQ/h = 5.53$ MHz, $\eta_Q = 0.219$, $\delta_{iso} = 12\,500$ ppm, $\delta_{CSA} = 700$ ppm, $\eta_{CS} = 0.36$, and a relative orientation of the quadrupole and shielding tensors $(\alpha, \beta, \gamma) = (7°, 8°, 333°)$. Figure 5(a) shows a two-dimensional ^{59}Co STMAS NMR spectrum of $Co(acac)_3$, recorded at $B_0 = 9.4$ T. Three distinct areas of signal intensity are observed. Lying along the $+1$ diagonal is an autocorrelation peak resulting from central transitions (CT) evolving in both the t_1 and t_2 periods. This CT$\rightarrow$CT signal is a characteristic feature of STMAS spectra, as this coherence transfer step cannot be canceled by phase cycling. The other two areas of signal intensity correspond to correlations involving the inner $\pm 3/2 \leftrightarrow \pm 1/2$ (ST_1) and middle $\pm 5/2 \leftrightarrow \pm 3/2$ (ST_2) satellites in t_1, with the central transition in t_2. From Eqs. (23) to (25) it follows that these $ST_1 \rightarrow$CT and $ST_2 \rightarrow$CT correlations will yield "ridge" line shapes with gradients of $+28/45$ and $-23/45$. Peaks with these slopes can be seen in the spectra, but it is also clear that these ST$\rightarrow$CT transitions exhibit a considerable broadening and splitting in the satellite (δ_1) dimension. These splittings arise from the cross term between the ^{59}Co quadrupole and CSA interactions. Similar splittings can be observed in STMAS NMR spectra recorded with a static magnetic field strength of 4.7 T [Fig. 5(b)]. The reduction in the number of central-transition sidebands owing to the

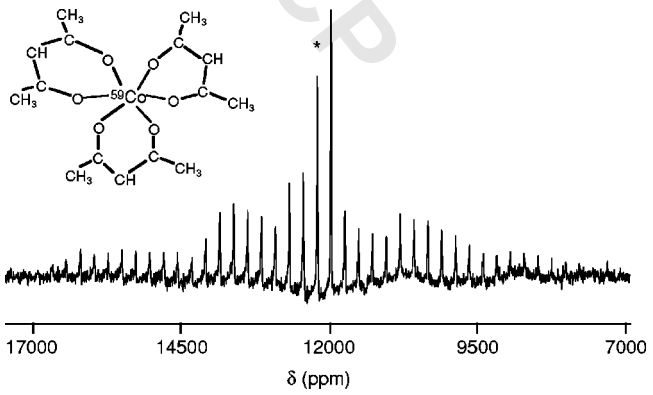

FIG. 4. Structure of cobalt(III)acetylacetonate, $Co(acac)_3$, and corresponding ^{59}Co NMR single-pulse spectrum resulting from averaging 48 transients with a recycle interval of 1 s. The MAS rate was 22.2 kHz and the position of the centerband is indicated by an asterisk.

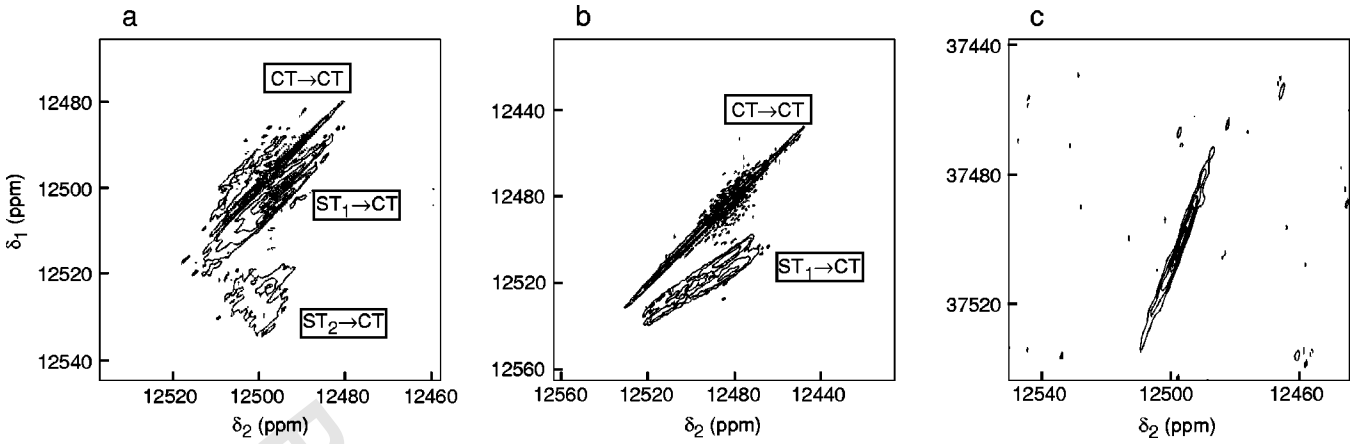

FIG. 5. Two-dimensional ^{59}Co STMAS NMR spectra of Co(acac)$_3$ recorded at static magnetic field strengths of 9.4 T (a) and 4.7 T (b). Other parameters: 640 (a) and 960 (b) transients per t_1 increment, 128 (a) and 96 (b) t_1 increments of duration 50 μs (a) and 100 μs (b), MAS rates of 20 kHz (a) and 10 kHz (b). A recycle interval of 1 s was used in each case. The two-dimensional ^{59}Co triple-quantum MAS NMR spectrum of the complex (c), recorded at a static magnetic field strength of 9.4 T under similar conditions to (a) (864 transients averaged for each of 96 t_1 increments), lacks the STMAS quadrupole-shielding splittings.

lower B_0 field strength results now in a better centerband intensity, and even though no ST$_2$→CT transfer is observed at the conversion pulse duration employed, the splitting in the ST$_1$→CT peak is evident. By contrast, no such splittings are observed in the 3QMAS NMR spectrum of this compound [Fig. 5(c)].

A better appreciation of the ST$_1$→CT quadrupole-shielding splittings can be obtained from the high-resolution projections arising upon summing the two-dimensional data orthogonal to the +28/45 ridge. Figure 6 shows the results of calculating such sheared projections of the 9.4 and 4.7 T STMAS data given in Fig. 5. The former yields a doublet split by approximately 200 Hz, whereas the latter reveals a very similar splitting (~220 Hz). This absence of a dependence of the splitting on the magnetic field strength is as expected from the quadrupole/CSA arguments given in Sec. III; indeed, line shapes obtained on the basis of Eq. (20) and of the parameters known for Co(acac)$_3$ yield a splitting of 203 Hz that is in very good agreement with these experimental traces (Fig. 6, simulation).

Equations (20) and (22) also predict that the second-order splitting resulting from quadrupole-shielding cross-term interactions will be larger for peaks arising from outermost ST$_2$→CT correlations. Figure 7 shows two-dimensional ^{59}Co STMAS NMR spectra of Co(acac)$_3$ recorded at static magnetic field strengths of 9.4 and 4.7 T, using pulse durations that have been optimized for such ST$_2$→CT transfers. Owing in part to the decreased excitation and conversion efficiencies associated with these middle satellite transitions, the signal-to-noise ratios in these spectra are poorer than in Fig. 5. Yet in both cases ST$_2$→CT peaks clearly display a considerable splitting centered around an axis of gradient −23/45. Spectra obtained from projections orthogonal to this axis are shown in Fig. 8; the splittings observed in these ST$_2$→CT peaks are again largely field independent (~620 and ~650 Hz, respectively), and in reasonable agreement with the splitting of 437 Hz expected from the theoretical arguments (Fig. 8, simulation).

V. CONCLUSIONS

The main purpose of this study was to present a comprehensive theory of higher-order quadrupole-shielding effects in solid-state NMR, and to demonstrate consequences of these effects in STMAS NMR spectroscopy of half-integer quadrupolar nuclei. For the ^{59}Co complex that was analyzed in this study, quadrupole-shielding cross terms appeared as splittings of the order of 10^2–10^3 Hz in the ST→CT peaks. Although from an experimental standpoint such broadenings may compromise the resolution of inequivalent sites achievable in STMAS experiments, these broadenings can also provide valuable information. To derive a formalism that allowed us to analyze such effects, an average Hamiltonian

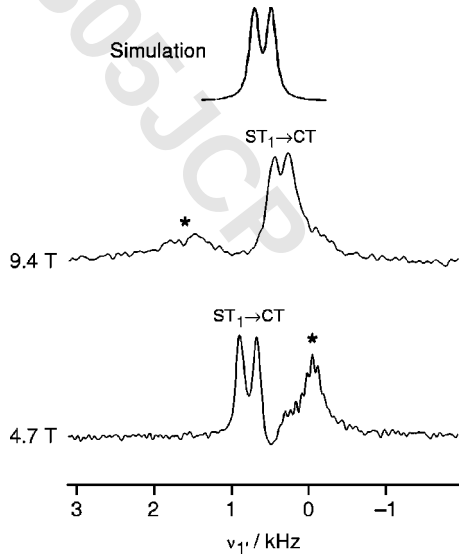

FIG. 6. Comparison between projections obtained from the two-dimensional ^{59}Co STMAS NMR spectra of Co(acac)$_3$ in Fig. 5 along an axis orthogonal to +28/45, and the field-independent prediction stemming from Eq. (18) for the known parameters of the compound. The simulation was convoluted with a 50 Hz line broadening.

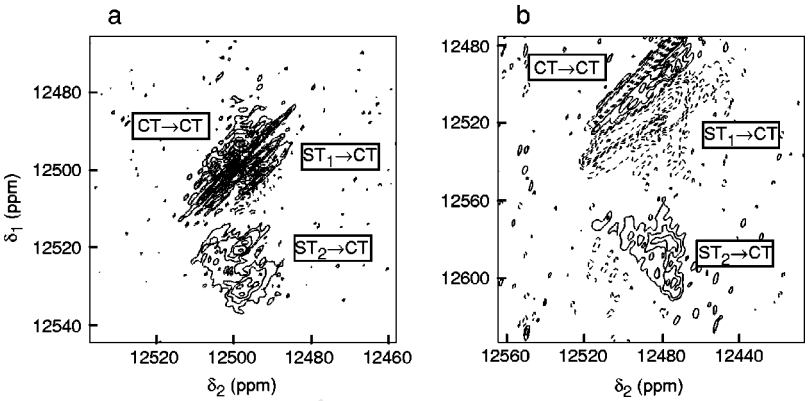

FIG. 7. Two-dimensional ^{59}Co STMAS NMR spectra of $Co(acac)_3$ optimized for $ST_2 \rightarrow CT$ transfer at static magnetic field strengths of 9.4 (a) and 4.7 T (b). Most acquisition parameters were as in Fig. 5 except for 1440 (a) and 1600 (a) transients per t_1 increment, 64 (a) and 32 (b) t_1 increments.

treatment valid in the high-field regime was employed. Specifying the MAS condition then resulted in simple analytical formulas describing the expected isotropic shifts. For the case of fairly well-resolved line shapes, a potentially useful feature of these cross-term effects is that they might allow extraction of the magnitude and relative orientations of quadrupole and shielding tensors, information that hitherto has required single-crystal studies,[36] complex multidimensional procedures,[37] or fittings of spinning sideband manifolds from random powders.[38] Also interesting is the manifestation of quadrupole-shielding effects as field-independent broadenings, as this enables their distinction from other broadening mechanisms arising from either shielding dispersions or from other types of second-order effects, which increase and decrease with B_0 strength, respectively.

It is worth concluding by noticing the connection that, from a spectroscopic standpoint, relates the quadrupole-shielding effects discussed in this work and the recently discussed quadrupole-driven reintroduction of dipolar couplings between quadrupolar and spin-1/2 nuclei.[39] Indeed, just like the chemical shift of the quadrupolar spin I, the dipolar coupling between I and any spin S may also be represented by a second-rank tensor capable of generating higher-order cross-correlations with the quadrupolar coupling of I. This will occur even if S is a spin-1/2 and, just as was the case with the CSA, the ensuing effect will show up as broadenings in the I-spin satellite transitions even under the action of MAS. Theoretical and experimental treatments similar to the ones developed in this study could then be used to detect such effects. Furthermore, analyzing the resulting line shapes in systems where the $I-S$ internuclear vector is known would have the added advantage of providing a molecular reference frame with respect to which to orient the I-spin quadrupole tensor. Efforts to detect such effects are currently under way.

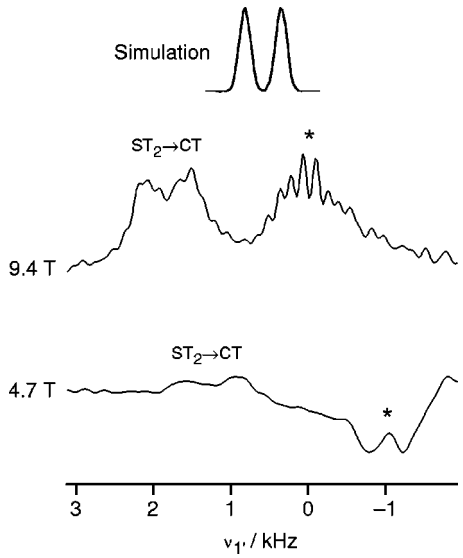

FIG. 8. Comparisons between the theoretically expected trace (top) and the experimental projections obtained from the two-dimensional spectra in Fig. 7 along an axis orthogonal to $-23/45$. Asterisks indicate the residual signals from the $ST_1 \rightarrow CT$ and $CT \rightarrow CT$ transitions.

ACKNOWLEDGMENTS

S.W. (USA) was supported by the US Department of Energy under contract no. DE-AC03-76SF00098. L.F. was supported by the US Department of Energy (Grant No. 00ER15049) as well as by the Philip M. Klutznick Fund for Research (Weizmann Institute). S.E.A. and S.W. (UK) acknowledge support from EPSRC (Grant No. GR/N07622) and are grateful to Dr J. McManus for preliminary theoretical work on quadrupole-shielding effects.

[1] P. J. Hore, *Nuclear Magnetic Resonance* (Oxford University Press, Oxford, 1995).
[2] M. Mehring, *High Resolution NMR in Solids* (Springer, Berlin, 1983).
[3] E. R. Andrew, A. Bradbury, and R. G. Eades, Nature (London) **182**, 1659 (1958).
[4] I. J. Lowe, Phys. Rev. Lett. **2**, 285 (1959).
[5] K. Schmidt-Rohr and H. W. Spiess, *Multidimensional Solid-State NMR and Polymers* (Academic, London, 1994).
[6] H. W. Spiess, in *NMR Basic Principles and Progress*, edited by P. Diehl, E. Fluck, and R. Kosfeld, (Springer, New York, 1978), Vol. 15.
[7] L. Frydman, Annu. Rev. Phys. Chem. **52**, 463 (2001).
[8] B. C. Gerstein and C. Dybowski, *Transient Techniques in NMR of Solids: An Introduction to Theory and Practice* (Academic, Orlando, 1985).
[9] D. Freude and J. Haase, NMR Basic Principles Progress **29**, 1 (1993).
[10] C. J. Groombridge, R. K. Harris, K. J. Packer, B. J. Say, and S. F. Tanner, J. Chem. Soc. Chem. Commun. ■, 174 (1980).
[11] A. C. Olivieri, L. Frydman, and L. E. Diaz, J. Magn. Reson. (1969-1992) **75**, 50 (1987).
[12] R. K. Harris and A. C. Olivieri, Prog. Nucl. Magn. Reson. Spectrosc. **24**, 435 (1992).
[13] S. Wi and L. Frydman, J. Chem. Phys. **116**, 1551 (2002).
[14] H. J. Jakobsen, H. Bildsøe, J. Skibsted, and T. Giavani, J. Am. Chem. Soc. **123**, 5098 (2001).
[15] Z. Gan, J. Am. Chem. Soc. **122**, 3242 (2000).
[16] Z. Gan, J. Chem. Phys. **114**, 10845 (2001).
[17] S. Wi and L. Frydman, J. Chem. Phys. **112**, 3248 (2000).
[18] L. D. Landau, *Quantum Mechanics* (Pergamon, Oxford, 1991).

[19] U. Haeberlen, in *Advances in Magnetic Resonance*, edited by J. S. Waugh (Academic, New York, 1976).
[20] E. W. Wooten, K. T. Muller, and A. Pines, Acc. Chem. Res. **25**, 209 (1992).
[21] B. F. Chmelka and J. W. Zwanziger, NMR Basic Principles and Progress **33**, 79 (1994).
[22] Z. Gan and D. M. Grant, J. Magn. Reson. (1969-1992) **90**, 522 (1990).
[23] L. Frydman and J. S. Harwood, J. Am. Chem. Soc. **117**, 5367 (1995).
[24] A. Medek, J. S. Harwood, and L. Frydman, J. Am. Chem. Soc. **117**, 12779 (1995).
[25] J. Mason, Chem. Rev. **87**, 1299 (1987).
[26] G. Wu and K. Yamada, Chem. Phys. Lett. **313**, 519 (1999).
[27] J. McManus, R. Kemp-Harper, and S. Wimperis, Chem. Phys. Lett. **311**, 292 (1999).
[28] S. Wi, V. Frydman, and L. Frydman, J. Chem. Phys. **114**, 8511 (2001).
[29] J. McManus, Ph.D. thesis, University of Exeter, 2001.
[30] E. Meirovitch and R. Poupko, J. Phys. Chem. **82**, 1920 (1978).
[31] Z. Gan, J. R. Quine, P. Srinivasan, S. Steuernagel, and B. Knott, poster W/T 061, 43rd Experimental NMR Conference, Asilomar, CA, 2002.
[32] K. J. Pike, S. E. Ashbrook, and S. Wimperis, Chem. Phys. Lett. **345**, 400 (2001).
[33] S. E. Ashbrook and S. Wimperis, J. Magn. Reson. **156**, 269 (2002).
[34] D. Massiot, B. Tonzo, D. Trumeau, J. P. Coutures, J. Virlet, P. Florian, and P. J. Grandinetti, Solid State Nucl. Magn. Reson. **6**, 73 (1996).
[35] K. Eichele, J. C. C. Chan, R. E. Wasylishen, and J. F. Britten, J. Phys. Chem. A **101**, 5423 (1997).
[36] T. Vosegaard, I. P. Byriel, L. Binet, D. Massiot, and H. J. Jakobsen, J. Am. Chem. Soc. **120**, 8184 (1998).
[37] A. Medek, J. R. Sachleben, P. Beverwyk, and L. Frydman, J. Chem. Phys. **104**, 5374 (1996).
[38] J. P. Amoureux, C. Fernandez, L. Carpentier, and E. Cochon, Phys. Status Solidi A **132**, 461 (1992).
[39] G. Wu and R. E. Wasylishen, Mol. Phys. **95**, 1177 (1998).